Low temperature reaction kinetics inside an extended Laval nozzle: REMPI characterization and detection by broadband rotational spectroscopy

Shameemah Thawoos[1], Nicolas Suas-David[2,*],

Ranil M. Gurusinghe[1,3], Matthew Edlin[1], Abbas Behzadfar[1], Jinxin Lang[1], and Arthur G. Suits[1,*]

[1] *Department of Chemistry, University of Missouri, Columbia, MO, 65211 USA*

[2]*Univ Rennes, CNRS, Institut de Physique de Rennes - UMR 6251, F-35000 Rennes, France*

[3]*Department of Chemistry, Tennessee Tech University, Cookeville, TN 38505 USA*

Chirped-Pulse Fourier-Transform millimeter wave (CP-FTmmW) spectroscopy is a powerful method that enables detection of quantum state specific reactants and products in mixtures. We have successfully coupled this technique with a pulsed uniform Laval flow system to study photodissociation and reactions at low temperature, which we refer to as CPUF ("Chirped-Pulse/Uniform flow"). Detection by CPUF requires monitoring the free induction decay (FID) of the rotational coherence. However, the high collision frequency in high-density uniform supersonic flows can interfere with the FID and attenuate the signal. One way to overcome this is to sample the flow, but this can cause interference from shocks in the sampling region. This led us to develop an extended Laval nozzle that creates a uniform flow within the nozzle itself, after which the gas undergoes a *shock-free secondary expansion* to a cold, low pressure conditions ideal for CP-FTmmW detection. Impact pressure measurements, commonly used to characterize Laval flows, cannot be used to monitor the flow within the nozzle. Therefore, we implemented a REMPI (resonance-enhanced multiphoton ionization) detection scheme that allows the interrogation of the conditions of the flow directly inside the extended nozzle, confirming the fluid dynamics simulations of the flow environment. We describe the development of the new 20 K extended flow, along with its characterization using REMPI and computational fluid dynamics. Finally, we demonstrate its application to the first low temperature measurement of the reaction kinetics of HCO with O_2 and obtain a rate coefficient at 20 K of $6.66 \pm 0.47 \times 10^{-11}$ cm^3 $molec^{-1}$ s^{-1}.

Email: nicolas.suas-david@univ-rennes.fr; suitsa@missouri.edu

Introduction

Reaction rate measurements at low temperature are important for practical applications such as modeling atmospheric and astrochemical environments, as well as for fundamental understanding of intermolecular interactions and reactivity generally. Much of what has been learned, particularly at low temperatures relevant to interstellar clouds, has derived from the pioneering work of Rowe and coworkers at Rennes. Beginning in the 1980's, they developed the CRESU method (French acronym for "Reaction Kinetics in Uniform Supersonic Flows)" in which reactions are studied in a collimated flow generated by a carefully designed convergent-divergent Laval nozzle[1, 2]. These flows are produced for a particular gas and a specific temperature and pressure and give rise to a cold, uniform reaction environment at densities of 10^{15}-10^{18} cm^{-3} without walls. Reactions have been studied at temperatures from over 160 K down to 6 K using the CRESU technique, and the method has been implemented with variations in laboratories around the world[3-9]. The original experiments employed continuous flows, and some at Rennes continue to do so, although these can consume enormous quantities of gas. In 1995, Atkinson and Smith first reported a pulsed version of CRESU, and most such instruments around the world now employ pulsed flows in which the gas consumption and pumping speed requirements are greatly reduced[10].

Pulsed flows are well-suited to the use of pulsed photolysis lasers to initiate reaction as is commonly the case. For detection, by far the large majority of CRESU experiments have followed Rennes in using laser-induced fluorescence (LIF). LIF has many advantages for CRESU application: it is extremely sensitive, tolerant of the high densities of the flow environment and quantitative. It is very useful for detecting certain important astrochemical radicals such as CN and OH[11-16]. However, LIF has some shortcomings as well: It is applicable to a rather limited range of molecules; it cannot be employed in a multiplexed approach to detect several species simultaneously, and the usual implementation with pulsed UV dye lasers calls for scanning the delay to map out the kinetic time profile which can be time consuming. To expand the range of suitable targets and to monitor reaction products, Leone and Wilson adapted the method to incorporate photoionization/mass spectrometric detection[5, 9]. They studied ethynyl radical reactions with a variety of coreactants including O_2[17, 18], allene[19], propyne[20] and acetylene[21, 22] using both laser photoionization and tunable synchrotron radiation as probe. This is a nearly universal detection technique, but as mass spectrometry requires very low pressures, the flow had to be sampled prior to detection as we discuss further below. In recent years we have coupled two alternative detection methods with uniform supersonic flows. In one case, we combined continuous-wave cavity ringdown spectroscopy

in the near IR, "UF-CRDS", to study low temperature reactions of CN (v=1)[23, 24]. This has the advantage that we can record the complete kinetic trace during each ringdown as the latter is well-matched to the hydrodynamics time of the flow, a method termed SKaR, "simultaneous kinetics and ringdown."[24, 25] This makes for very rapid measurements so that a complete pseudo-first order study could be completed in an afternoon. The disadvantages are the limited spectral range (thus limited target reactant) possible for any given optical configuration and again the impossibility of multiplexed detection.

In 2014, in collaboration with the Field group at MIT, we first coupled the revolutionary new method Chirped-Pulse Fourier Transform millimeter Spectroscopy (CP-FTmmW) with uniform supersonic flows[26, 27]. CP-FTmmW permits a broad linear frequency sweep of many GHz at high power in each excitation pulse of a microsecond or so[28-30]. Detection then follows by monitoring the free induction decay (FID) of the coherence arising from any molecules excited by the chirp. This combination, which we termed CPUF for "chirped pulse/uniform flow" has many desirable features. There are thousands of resolution elements in each frequency sweep, and each molecule has a "fingerprint" spectroscopic pattern determined by its rotational constants, so that molecules can be identified at low signal levels within complex mixtures. It is a multiplexed approach: many species can be monitored simultaneously without difficulty, and these can be reactants or products or both at once[31, 32]. Although the sensitivity of rotational spectroscopy is inferior to LIF, the large interaction volumes and high density of the flows can compensate. The flow is an ideal environment for rotational spectroscopy in that many collisions with the carrier gas permit cooling to low rotational levels for detection. One serious challenge of the approach is that the high collision frequency in high-density flows can strongly attenuate the FID and greatly reduce the sensitivity. To overcome this, we developed a quasi-uniform condition in which a flow was established inside the nozzle at the pressure for which it was designed (or nearly so) after which a second expansion to low density and lower temperatures took place in the main chamber, ideal for CP-FTmmW detection[32]. This approach allowed us to make measurements of product branching in photodissociation and reaction for complex systems, as products could be formed, then cooled to the detected rotational transitions, but with imperfectly defined reaction conditions. Moreover, as the uniform portion of the flow was short-lived and not well-characterized experimentally, kinetics measurements could not be performed. These experiments were in a sense analogous to those studying reactions in Chen "hyperthermal" nozzles although at low temperature rather than high temperature[33, 34].

To perform kinetics studies, several hundred microseconds of uniform conditions are generally necessary. To achieve this while still employing CP-FTmmW detection, we recently adapted the technique of airfoil

sampling of the flow developed by Wilson and Leone at the ALS for use with CPUF[9, 35]. This permitted us to use the full flow condition for kinetics, then sample though a small orifice into a separate differentially pumped region for detection. We measured the rate coefficient for the reaction of CN with ethane at 50 K and found good agreement with previous CRESU measurements[35]. We also showed that photodissociation along the flow takes a "snapshot" of the density profile that then propagates into the detection region revealing any fluctuations. However, it is clear from simulations we and others have performed that shocks may occur in these environments, either just prior to sampling or just after, that can interfere with the measurements[35]. We have thus sought an alternative approach that is free of such shocks. We describe this alternative approach here. In this method we perform the reaction fully within an extended Laval nozzle, after which a second expansion to low temperature and pressure takes place at the exit of the extended nozzle where the mm-wave probe takes place. This is analogous to the quasi-uniform flow condition, albeit with a longer and actual uniform flow established within the nozzle. A challenge with this approach is that it is not possible to measure the flow conditions using the usual impact pressure measurements. Instead, we use resonant multiphoton ionization (REMPI) to record the rotational distribution for a very dilute sample of NO, with the electrons produced thereby captured by a series of electrodes embedded in the nozzle extension. We further show this very simple and sensitive REMPI detection can be used in the external flow and may offer an alternative probe scheme for atoms or other species with favorable REMPI schemes. Finally, we demonstrate application of the extended flow to measure the bimolecular rate coefficient for the reaction of formyl radical (HCO) with O_2 at 20 K. The kinetics of the radical-radical reaction of HCO with O_2 has been studied at room temperature and higher[36-39]. Here we report the first measurement of the rate coefficient for reaction of HCO with O_2 at 20 K.

Experiment Overview

The instrumentation for the CPUF experimental setup used has been presented elsewhere in detail[26, 27], therefore only a brief account will be given here. The schematic of the experiment is shown in figure 1(a). The experimental setup consists of two main components: the pulsed Laval flow and the chirped pulsed mm-wave spectrometer. In this report, except where otherwise noted we use variations on a 20 K helium nozzle to generate high density pulsed uniform flows at 2×10^{17} cm^{-3}. These flows are produced by a homebuilt high-throughput stacked piezo valve that supplies a 20 cm^3 reservoir at the nozzle entrance. The experiment typically operates at a 2-5 Hz repetition rate. For the He flow the valve is pulsed open for 3.5 ms at which time the reservoir pressure rises to 360 torr as measured by a Kulite pressure sensor. The

flow enters the main chamber which is a polycarbonate tube through which the mmWave radiation is directly broadcasted and collected. The chamber is pumped by two turbomolecular pumps and supplied N_2 slip gas as needed to bring the chamber pressure either to the target pressure for the uniform flow, 0.5 torr, or by varying the repetition rate and eliminating the slip gas, to 0.02 torr to permit a second expansion as discussed further below. The gas mixtures are supplied to the pulsed valve by several mass flow controllers in parallel.

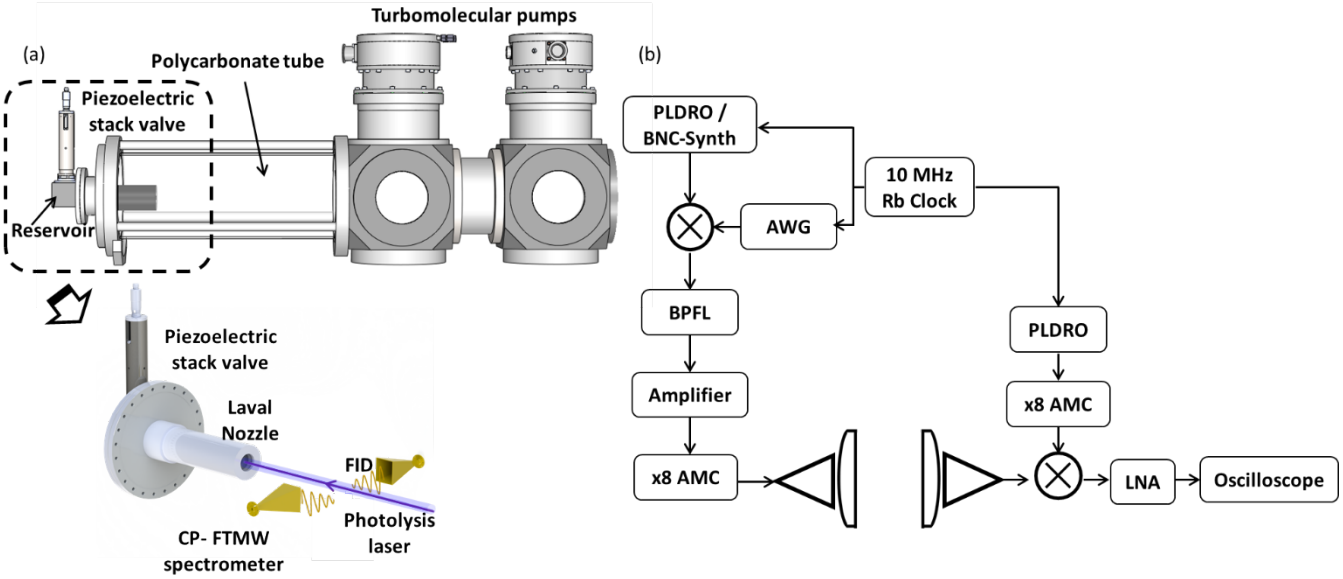

Figure 1 (a) Schematic of the CPUF instrumentation. (b) Components of the mmWave spectrometer.

The mmWave spectrometer has been previously described in detail and is employed in a variety of configurations. In this instance, schematically shown in Fig. 1(b), signals from an arbitrary waveform generator (AWG7082C, Tektronic) were mixed with a frequency of 8.125 GHz using either a phased locked dielectric resonator oscillator (PLDRO) or a low-noise microwave synthesizer (BNC-model 845-M) via a double balanced mixer (Marki M10418LC). The output of the mixer was filtered through a matched bandpass filter and sent through an amplifying stage to an active frequency multiplier chain (AMC, QuinnStar Technology, QMM-751020080), where the signal is multiplied by 8 to obtain the desired frequency within the range of 80-90 GHz. The resulting frequency was broadcast using a standard gain horn. The output of the horn was focused using a 150 mm focal length (Thorlabs) plano convex PTFE lens and into the polycarbonate chamber set perpendicular to the Laval flow, as shown in Fig. 1(a). The free induction decay (FID) of the excited molecules was collected via a receiving horn and down-converted by mixing (Millitech, MXP-12-RFSL) with a fixed frequency generated by a PLDRO at a fixed frequency of 10.7

GHz using an AMC (Millitech, AMC-12-RFH0A) sent through an 8x AMC. The down-converted output of the mixer is amplified using a low-noise amplifier (LNA, Miteq AMF-4D-00100800-18-13P) and sent to the oscilloscope (Tektronic DPO70804C) where the data is visualized and averaged. All the microwave components are phased locked to a Rubidium clock at 10 MHz. The mmWave excitation is pulsed and the FID recorded 50 times in a burst mode for each gas pulse. The mmWave pulses, 1 μs long, are spaced 5 μs apart and the resulting FID is Fourier transformed using a 400 ns gate with a Kaiser-Bessel window function to obtain frequency domain spectra at 5 μs intervals up to 350 μs. This permits recording the full time-dependent kinetics for each gas pulse. The photolysis laser, an ArF 193 nm excimer (Coherent COMPEX PRO 205F) employing unstable resonator optics, is fired 11.8 μs after the first mmWave pulse. The excimer beam is well-collimated with a 4 mm $\times$ 20 mm rectangular profile and is not focused.

For determination of the rotational temperature, NO 1+1 REMPI is employed on the (0-0) band of the A-X transition around 44200 cm^{-1}. The probe laser is a Sirah Cobra Stretch operating on Pyridine 1 dye at 678 nm pumped by a Quanta-Ray Nd:YAG laser at 532 nm. The dye output is doubled then mixed with the fundamental in a beta barium borate crystals to give the desired UV radiation. For these measurements the UV is attenuated to very low power to avoid heating the plasma as discussed below.

Results and Discussion

REMPI detection in the uniform flow

We first demonstrate REMPI detection directly in the flow, as shown schematically in Fig. 2. We have employed two different flows, one from a 3D printed nozzle designed for an Ar flow at ~50 K and the other is a machined aluminum nozzle producing a ~30 K flow with neon gas. For these measurements the instrumentation was modified by removing the polycarbonate chamber as shown in Fig. 2(a). The large stainless-steel Tee that holds our first turbopump has access ports for the laser which allowed the ionization laser to be aligned perpendicular to the Laval flow. We used a variation of the strategy employed by Cool and coworkers to monitor REMPI signals in flames, shown in Fig. 2(b)[40, 41].

We suspended two copper gaskets with inner and outer diameters of 6.00 and 6.75 inches, respectively, around the flow spaced by 6 cm. These copper rings served as cathodes held in the range of -300 to -370 V. We used a simple collector wire as the anode, just below and downstream of the laser crossing region, which was 20 cm downstream from the nozzle, to capture the emitted electrons. The collector was grounded through a 125 kΩ resistor with the two leads connected directly to an oscilloscope feeding a LabVIEW data acquisition program that could integrate and average the oscilloscope signals as the laser was scanned. The signals were quite strong, and no amplification was required. We found it necessary to reduce the total ionization yield dramatically to prevent the plasma from heating the flow locally giving an artificially high rotational temperature. This required reducing the probe laser power to levels below

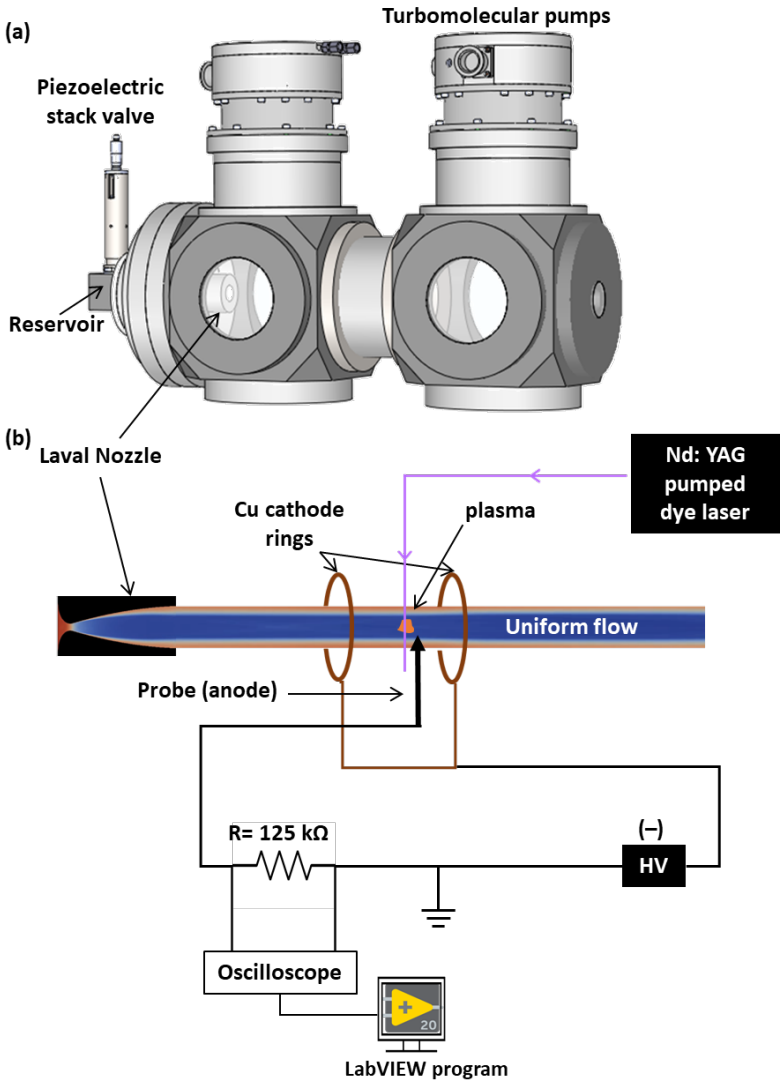

Figure 2 (a). Schematic of the modified CPUF instrumentation facilitating REMPI detection. (b). Schematic representing the REMPI detection scheme.

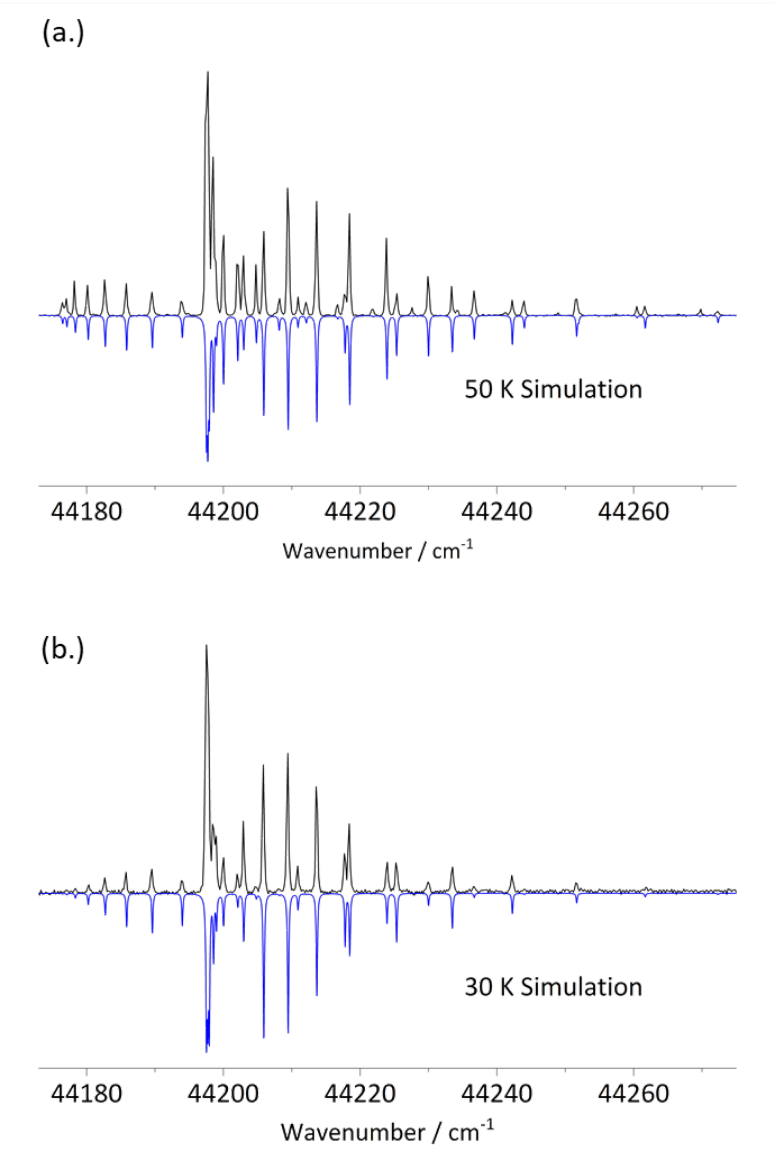

Figure 3. Rotationally resolved 1+1 REMPI spectra of dilute sample of NO in 50 K Ar flow (a) and 33 K neon flow (b). The experimental spectra are in black, and the simulated spectra obtained using LIFBASE are inverted and in blue.

120 μJ/pulse and at the same time lowering the NO density in the flow to less than ~3.0×10^{13} and 2.0×10^{14} molecule cm^{-3} for the 33 K and 50 K flow respectively. The obtained spectra are compared with LIFBASE[42] simulations and reasonable agreement is found between the flow temperatures inferred from fitting the REMPI scans and those obtained by impact pressure measurements of the nozzle (here the kinetic temperature is assumed to be equal to the rotational temperature) Fig. 3. We thus demonstrated the ability of NO REMPI to monitor conditions directly in a high-density uniform flow. Application of this approach for 2+1 REMPI to detect atoms or other molecules in the flow, and performance following the

introduction of a photolysis laser will clearly be more challenging than NO detection. These are the subject of ongoing investigations.

Extended Laval nozzle

As mentioned in the Introduction, probing a supersonic uniform flow with CP-FTmmW is not trivial, as the relatively high pressure of such an expansion is not compatible with the probing approach. Previous setups, mostly relying on mass spectrometers[5, 9, 43], overcame this difficulty by sampling the flow through a skimmer or airfoil associated with a secondary chamber[44]. Except when dealing with ionized gas, any obstacle placed within the supersonic flux produces a shock along the flow pathway. A shock layer associated with a sharp increase in temperature and density may be harmful to kinetic measurements. A skimmer cannot eliminate the clogging effect at the entrance of the secondary chamber. At best, a well-designed skimmer could significantly reduce the strength of shock, but its use in the lab comes with other technical complications. Indeed, in addition to recourse to an additional chamber and pump system, the profile of the skimmer is optimal for a unique Mach number. Thus, to effectively attenuate shock, a skimmer should be built along with the corresponding Laval nozzle. Even under these optimal conditions, a numerical study is necessary to gain insight into the strength of the shock, as no current experimental characterization approach allows an accurate description of the flow structure within the narrow skimmer.

The recourse to the extended Laval nozzle overcomes the drawbacks of the sampling methods. First, this new approach simplifies the experimental setup because no secondary chamber, additional pump system, or skimmer design is required. Second, it is a shock-free approach that removes the challenges of dealing with possible data corruption by the presence of a shock layer before probing the expansion.

To better understand the principle behind the extended nozzle, the CFD simulations presented in Fig. 4a-d present the different steps described hereafter culminating in the extended nozzle design in Fig. 4d. We first consider a simple extension as shown in Fig. 4b. Here, a cylindrical tube matching its final diameter is added to a conventional Laval nozzle at its output where the uniform flow normally propagates in a wall-free environment. Then, instead of the chamber pressure set to match the flow pressure, the former is decreased as much as possible to produce an under-expanded free jet where the temperature and pressure are much lower (suitable for CP-FTmmW measurements) than the initial uniform flow from

which it originates. Being supersonic, the flow within the extended tube is not influenced by the upstream conditions of the vacuum chamber (low pressure). Thus, while the pressure conditions surrounding the isentropic core do not fluctuate, the flow remains well-collimated. However, owing to the interaction of the gas with the wall, the boundary layer increases along the tube, increasing the pressure around the isentropic core. In turn, the isentropic core shrinks, triggering a diamond shock structure associated with large fluctuations in thermodynamic parameters. To compensate for the boundary layer increase, the divergent profile of the extended tube must be calculated as described in the following.

Profile of the extended Nozzle

To preserve the established isentropic core, the evolution of the boundary-layer thickness must be considered. As a constant mass flow is essential for maintaining high-quality expansion, we turn to the displacement thickness concept to retrieve the profile that will not affect the isentropic core. This approach relies on the integral method of Cohen and Reshotko[45], where the wall shear stress, heat transfer, and transformed freestream velocity are dimensionless parameters. The implementation follows the work of Potter and Carden[46] in which the different steps and iterations are discussed. As a uniform flow is already fully established, the iterative process becomes much simpler than that for designing the nozzle. In particular, the correlation number linked to the pressure gradient is null, allowing a more direct calculation of the momentum thickness and shape factor, and thus, the definition of the displacement thickness. In the present case, the increase in the diameter of the extended tube was treated simply using a linear divergence angle of 2 ° (Fig 4 c and d).

CFD simulation of the extended Laval nozzle

The newly calculated profile of the extended tube was numerically characterized by computational fluid dynamics (CFD) using the open-source library OpenFOAM v11[47, 48]. The temperature, density, and velocity distributions are computed using the time-dependent density-based solver shockFluid, which is well-suited for modelling high Mach number flows. The structured mesh was composed of 120000 quad cells with a side length of approximately 300 µm. This mesh takes advantage of cylindrical symmetry, where the 3D nozzle is reduced to a less computationally expensive 2D wedge-shaped slice with a 0.5° angle. Apart from the symmetry condition normal to the flow propagation, the mesh was limited by three types of boundary conditions: the inlet to which the total pressure end temperature was set, the no-slip wall of

the nozzle, and the total pressure of the chamber to mimic the vacuum produced by the pump system associated with the condition to avoid unrealistic back reflections from the high Mach number expansion.

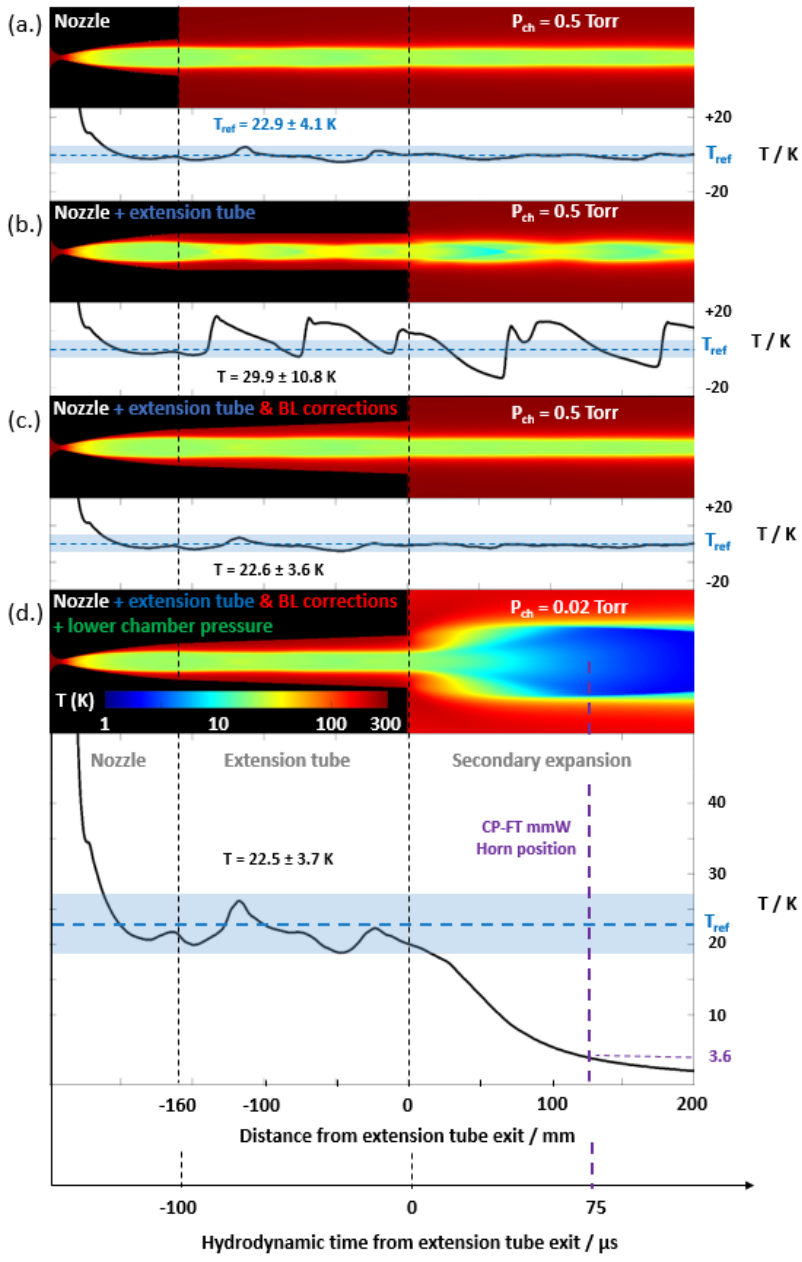

Figure 4. Evolution (1D and 2D) of the temperature in four different nozzle configurations: default nozzle (a) combined with a fixed diameter extension (b) and divergent extension tube (c). The latter (c) produces a flow analogous to that of the default nozzle, and when the chamber pressure lowered (d), produces an underexpanded free jet suitable for CP-FTmmW measurements.

The numerical characterizations are shown in Figure 4. Along with the extended nozzle used in this study (Fig. 4 d), figures 4a to 4c give the reader an intuitive representation of the different steps that lead to its design. The original nozzle (Fig. 4a) produces an optimal uniform flow, whereas the adjunction of a simple cylindrical extension tube (with a fixed diameter) leads to a flow with large fluctuations in temperature and density (Fig 4 b). In contrast, the extended tube associated with the 2° divergent profile (Fig 4 c) led to an expansion similar to that of the nozzle alone (Fig. 4 a). Finally, by decreasing the chamber pressure, the flow inside the extended tube was largely preserved, but an underexpanded free jet appeared in the chamber, characterized by a lower temperature and density suitable for the CP-FTmmW detection (Fig. 4 d). The reference temperature shown (T_{ref}) is that determined by CFD of the original nozzle profile. It is largely preserved

even in the extended nozzle with secondary expansion: the average temperature of the simulation in that case is 21.1 ± 3.4 K.

Characterization of the flow within the extended nozzle

The CFD results in Fig. 4 show promise for application to CRESU-style studies but the usual means of monitoring the flow conditions, i.e., impact pressure measurements, are likely not feasible inside the

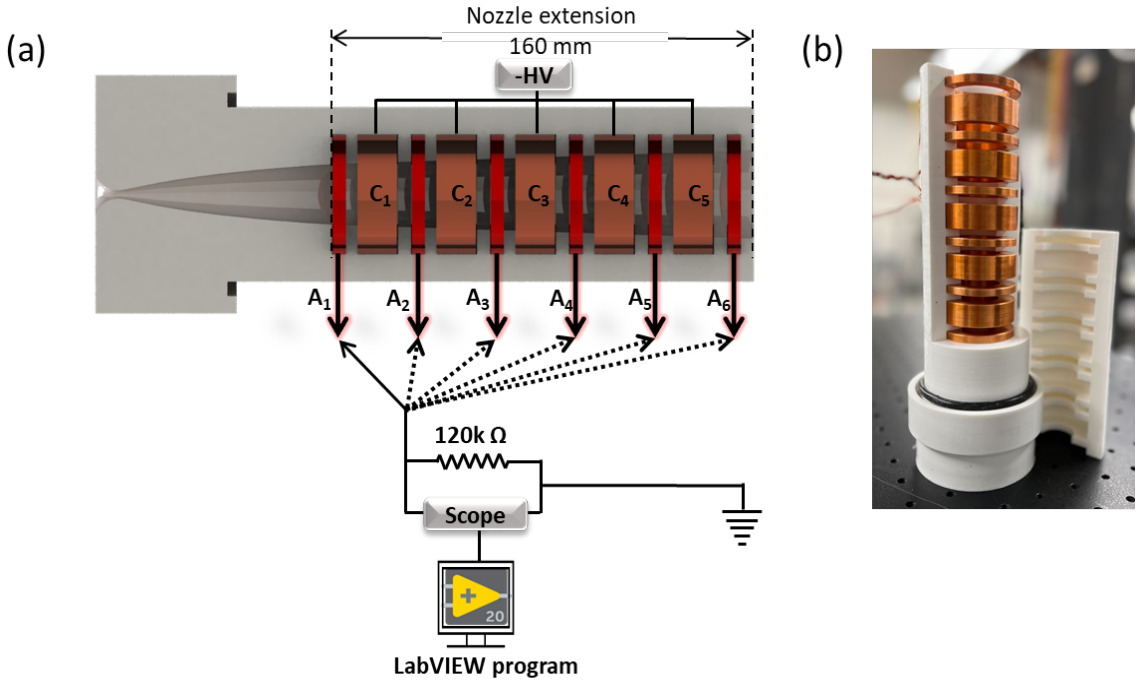

Figure 5 (a) Schematic of the extended Laval nozzle and the REMPI detection electrodes placed within the nozzle extension. (b) A picture of the 3D printed nozzle extension and the copper electrodes housed in it.

nozzle owing to shock waves that could be produced by the pitot probe itself. Instead, we have opted to adapt our REMPI detection within the nozzle. To this end, we have constructed a nozzle that includes a series of copper electrodes embedded in a conical extension to the nozzle as shown in Fig. 5. This consists of six anodes that are 5 mm thick alternating with five 15 mm thick cathodes. These are housed in a split 3D printed extension assembly, and both the electrode inner diameters and the nozzle extension are shaped so that upon assembly, the inner profile is a smooth conical extension to the original nozzle as modeled in Fig. 4c and d. For the REMPI measurements, the unfocused probe laser is sent counterpropagating to the flow with the cathodes are held at -250 V. We performed SIMION simulations (Fig. 6) to confirm that the electrons collected on a given anode originate from the region between the surrounding cathodes and not elsewhere. For this simulation we used a cylindrical distribution of electrons

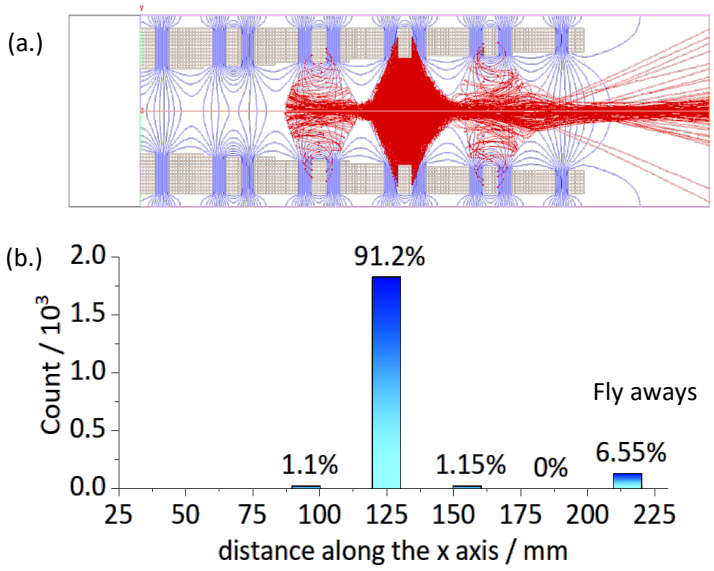

Figure 6 (a) SIMION simulation and calculated trajectories (red solid lines) for electrons originating from the region between the midpoints of the cathodes surrounding anode A_4. Equipotential contours are shown in blue. (b) Histogram of electron counts with respect to the electron impact position.

roughly matching the probe laser diameter and extending from the midpoint (along z) of one cathode to the midpoint of the next. The initial electron kinetic energy was chosen to match the maximum available from the 1+1 REMPI process and given a uniform spherical angular distribution of emission. The simulation showed that > 90% of the electrons are recorded on the intended anode with very few leaking to neighboring sites, with 6% "fly aways," those escaping from the nozzle entirely. The SIMION results thus confirm that each anode is reporting on the distinct local environment.

We then used these electrodes to record the NO rotational distribution as above, recording the spectrum from each anode in sequence. The conditions in this case were as follows: the supplied gas was helium with ~300 ppm NO; laser power was < 120 μJ/pulse (lower than the minimum detection limit of the laser power meter, Ophir PE50BF-C); reservoir pressure was 360 torr, and chamber pressure ~2 × 10^{-2} torr. Scans were recorded at 0.01 cm^{-1} per minute at 2.5 Hz after dividing the laser frequency by four and 4 pulses were averaged for each point. Electron signals were integrated for 200 μs after each laser pulse. The results obtained for each anode are shown in Fig. 7 along with temperature obtained from the fits simulated using LIFBASE while minimizing residuals. We estimate the uncertainty in each fit as $\pm$ 1.6 K based on the variation of the chi squared value around the minimum. The results gave flow temperatures from 17 to 21.5 K with an average of 19.7 K, in good agreement with the simulation and with the external flow determined by impact pressure from the original nozzle.

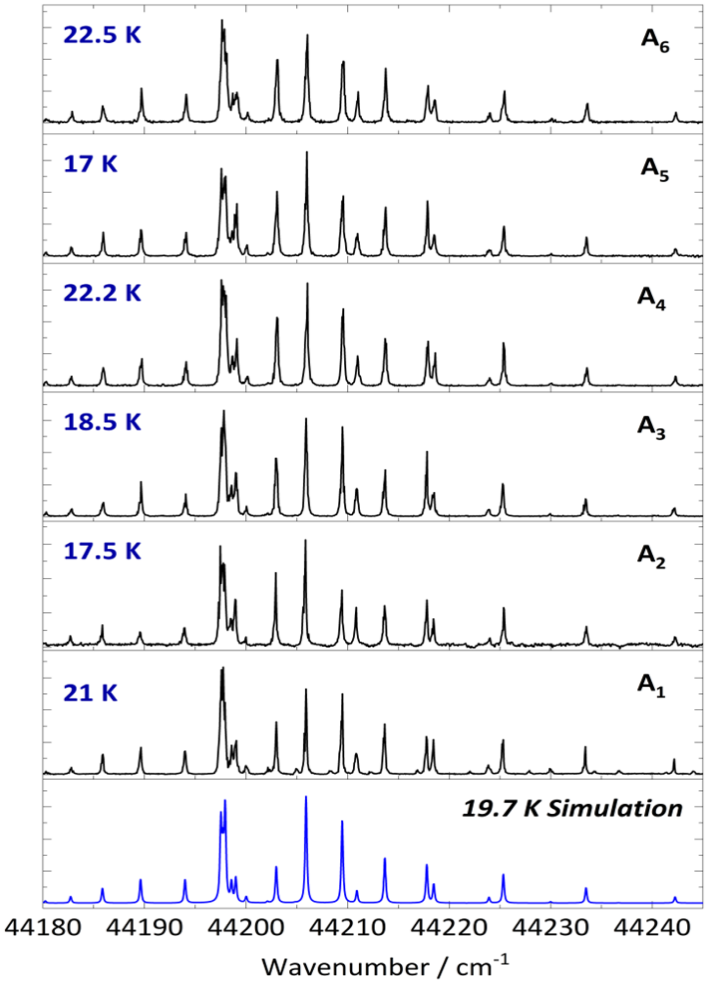

Figure 7. 1+1 REMPI spectra recorded at each anode (A_1-A_6) and the LIFBASE simulation (Blue).

As the REMPI approach experimentally confirmed the feasibility of using an extension tube for the Laval nozzles, subsequent extended nozzles could be validated through Pitot measurements by checking the presence of a uniform flow in the vacuum chamber kept at the expected pressure for the nozzle used.

The secondary expansion

It is also of interest to monitor the conditions of the secondary expansion. In this case we can use both REMPI measurements and rotational spectroscopy to do so. We first configured a small detector to monitor the temperature in the secondary expansion, shown in Fig. 8(a). This detector used a different configuration from that in our initial experiments shown in Fig. 3 as here the laser propagates counter to the flow, and we wish to restrict the origin of the captured electrons to the region near the collector. The measurement here, shown in Fig. 8 (b), gave a rotational temperature for NO of ~5 K at a position 13.5 cm downstream from the exit of the nozzle.

We then used CP-FTmmW measurements using furan broadband scans from 88680 MHz to 88780 MHz comprising rotational lines J = 5, 9, 10 and 11 whose relative intensities are quite sensitive to the temperature in the range of 3 - 15 K. There are also higher J lines nearby suitable for 10-30 K that make furan a convenient temperature probe in this frequency region. We measured the rotational distributions at a series of distances of the spectrometer horns downstream of the nozzle exit. We fitted the results

using PGOPHER[49] with rotational constants from The Cologne Database for Molecular Spectroscopy (CDMS)[50] as shown in Fig. 9. The furan results ranged from 12.4 K at 7.5 cm to 3.9 K at 13.5 cm, the latter in good agreement with the REMPI measurement made at the same position.

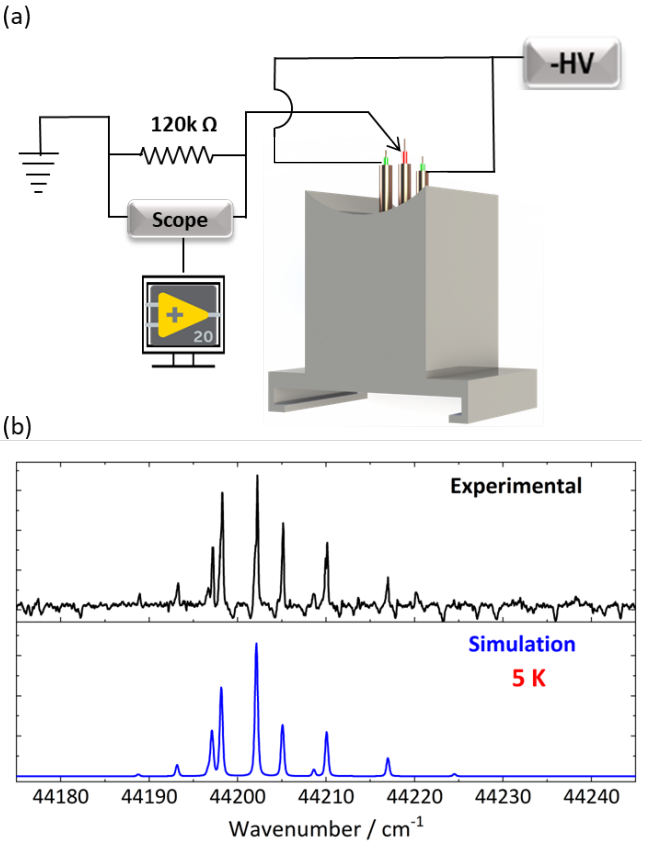

Figure 8 (a). REMPI detector to monitor electron current in the probe region. (b) Experimental (black) 1+1 REMPI spectra of NO in the secondary expansion at 13.5 cm from the exit of the extended nozzle and theoretical (blue) simulation using LIFBASE.

We can also use characterization of the FID rate to provide insight into the collisional interruption of the coherent emission of excited molecules in the region of the secondary expansion. The modified Bloch equations have been widely used to interpret the FID after excitation and abrupt interruption. The time dependent FID signal ($S_{(t)}$), can take the form,

$$S_{(t)} \propto \exp(-t/T_1) \exp\left(-t/T_2\right) \cos(\omega t)$$

where ω is the transition frequency, t is the time, and T_1 and T_2 are phenomenological FID time constants[51-53]. T_1 relates to the thermal relaxation of the population difference, whereas T_2 relates to the dephasing of the coherence due to collisions, Doppler spread, and other processes. It is not readily possible to disentangle the two contributions as they have the same form; we assume the leading contribution at low temperature is from T_2. We measured T_2 by monitoring the FID decay signal. Because the recorded FID signal is very weak compared to the excitation mmWave pulse, we recorded the FID following the single-frequency excitation pulse and Fourier-transformed the signal using a short FT gate then scanned the gate across the FID signal. The resulting FT signal intensity with respect to the gate position is then fitted to an exponential decay to recover the T_2 time constant.

We used a 0.06% sample of furan with a single-frequency excitation pulse (88.757 GHz, overlapping 8_{16}-7_{17}/8_{26}-7_{27} transitions, for 1 μs duration) to excite the furan molecules, then recorded the FT signal up to

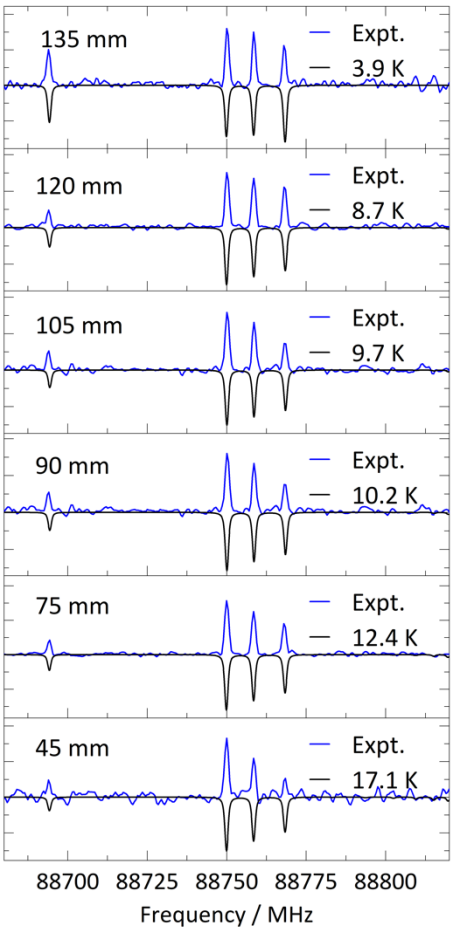

Figure 9. CP-FTmmWave spectra of 0.06% Furan in the flow (blue) at different distances from the exit of the extended nozzle and the PGOPHER simulation of furan done using rotational constants from CDMS database (black).

1300 ns. The measurement and results are shown in Fig. 10. We find lifetimes up to 50% longer with distance downstream, with T_2 reaching ~ 500 ns. This can be attributed mainly to the lower temperature hence lower collision frequency downstream, although slight decrease in pressure with distance likely also contributes to the lower collision frequency.

Figure 11 summarizes the theoretically calculated temperature along the flow axis and experimental determination of the temperature of the flow. The calculated temperature inside the isentropic core of the extended nozzle at higher chamber pressure conditions is 22.5 ± 3.0 K and remains closely similar to the previous Pitot measurements (not shown in this manuscript) performed on the original nozzle. The average temperature calculated from the CFD simulation within the extended nozzle with a secondary expansion is 21.1 ± 3.4 K and this agrees very well with the experimentally determined temperature obtained using 1+1 REMPI of NO sample 19.7 ± 2.5 K (Fig 11. Blue solid circles). Possibly owing to the gradient temperature along the line of sight close to the nozzle output, the temperatures retrieved by CP-FTmmW within the secondary expansion (Fig 11 solid red diamonds) are slightly higher than those calculated. At 135 mm downstream from the extension tube output where the horns are placed to perform kinetics measurement, the temperature retrieved by both the CP-FTmmW and REMPI approaches (3.9 and 5 K respectively) are very close to the temperature calculated through CFD (3.9 K).

CRESU inside the nozzle

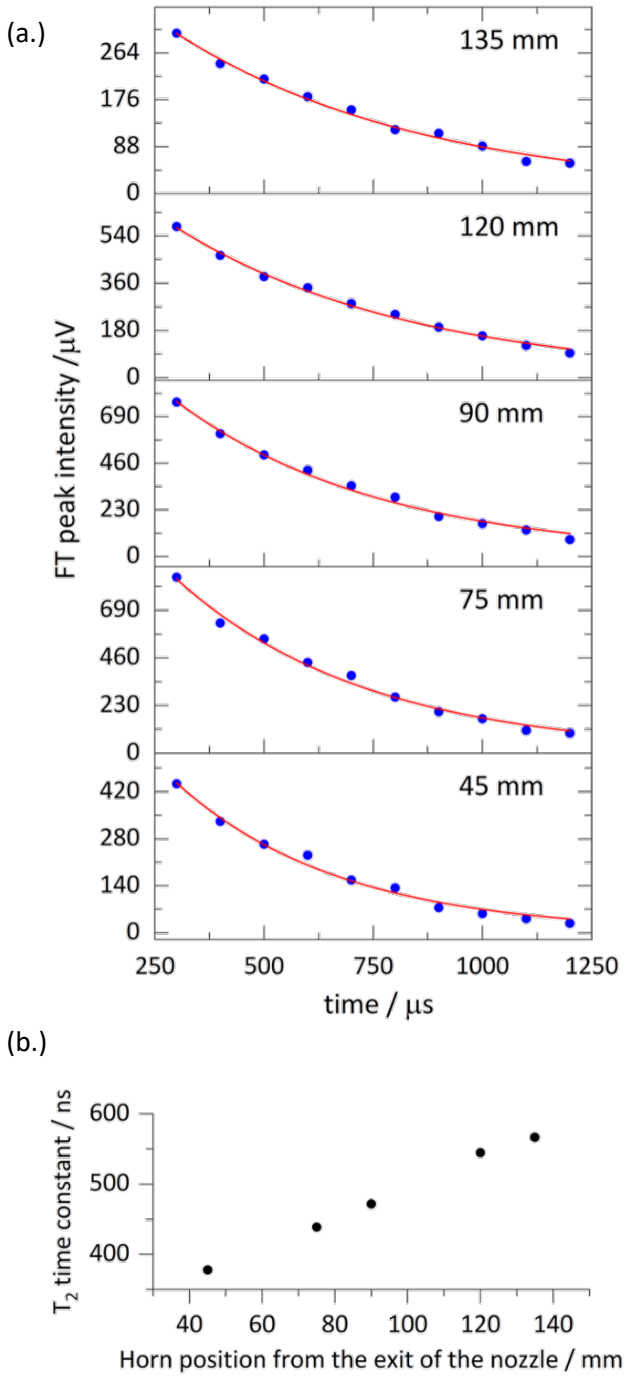

Figure 10. (a) FID signal vs FT gate position at different horn distances from the exit of the extended nozzle with single exponential fit, and (b) is the horn position vs the T_2 time constant.

Having established the uniform flow within the extended nozzle for more than 200 mm, we performed a low temperature kinetics measurement to illustrate the approach for CRESU. We choose the reaction of HCO with O_2:

$$HCO + O_2 \rightarrow HO_2 + CO$$

The experiments were carried out in pseudo-first order with respect to HCO. Furan was used as the precursor for HCO. The pseudo-first-order conditions used to study the reaction are listed in Table 1. Furan has a large absorption cross-section at 193 nm and produces HCO + propargyl radical (C_3H_3), likely through excited-state decay following S_2-S_1 internal conversion. Other channels include CO + C_3H_4 and CH_2CO + C_2H_2[54]. The branching between these various channels is not known, but they are present in low yields and do not interfere with the pseudo-first-order determination of the HCO decay rate dependence on O_2 density. HCO was monitored on the 1_{01}-0_{00} (3/2←1/2) transition at 86670.76 GHz. We used the Fast Frame mode of the oscilloscope to record 350 μs of signals for each gas pulse as described in the experimental section.

The time-dependent integrated line intensities are shown in Fig. 12 for various O_2

densities. The photolysis laser, with a laser fluence of approximately 32 mJ cm^{-2}, fires at 34.8 µs after the first mmWave pulse to initiate the reaction. The HCO signal starts appearing approximately 15-20 µs after

Table 1 Summary of experimental conditions for the reaction of HCO with O_2.

Flow			Photolysis laser flux / mJ cm^{-2}	[Furan] / 10^{14} molecule cm^{-3}	[O_2] / 10^{14} molecule cm^{-3}	No of measurements
Temperature / K	Gas	Density / 10^{17} molecule cm^{-3}				
19.7 ± 2.5	He	2.30	32	1.37	0.29-3.35	12

the excimer fires and has a steady rise till ~100 µs, which is equivalent to the passage of HCO from the nozzle exit through the secondary expansion to fill the probe volume. Following this rise, in the absence of the co-reactant, we observe that the HCO signal shows a slow rise signal for up to 225 µs, and then a steep increase followed by a sharp drop (Fig. 12(a)). The trend in the HCO signal intensity corresponds to each part of the flow. The steep rise appearing at later times corresponds to the dense flow within the

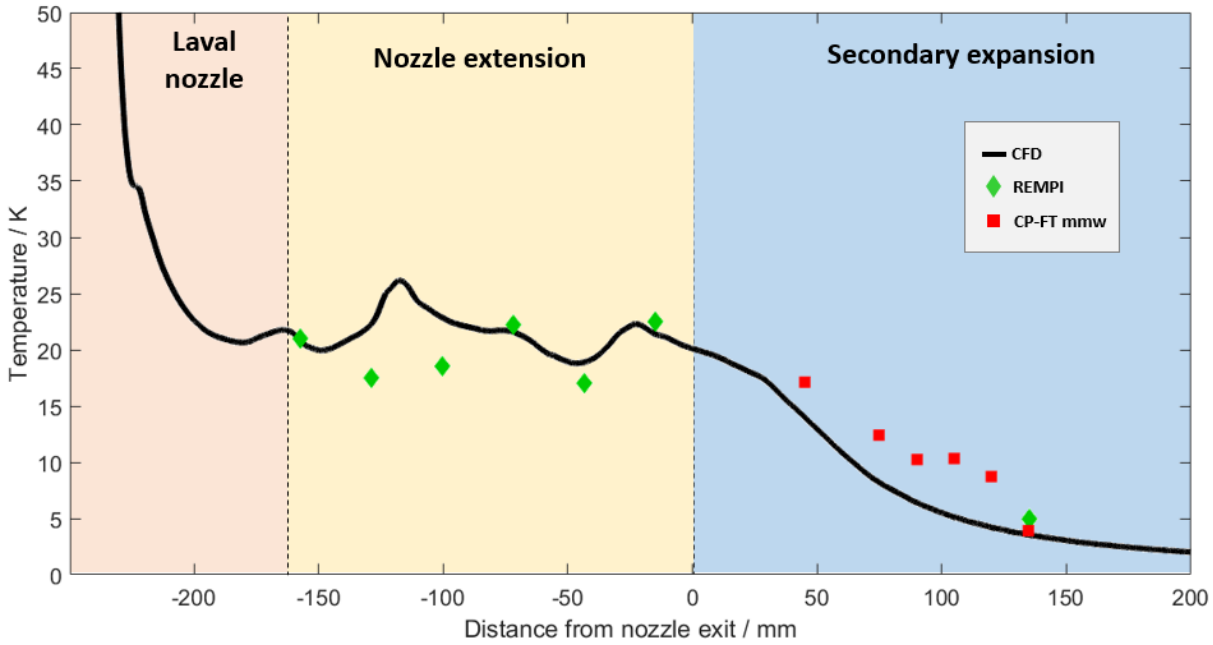

Figure 11. Comparison of theoretical and experimental temperature of the flow along the axis of the extended nozzle along with the underexpanded secondary expansion. Solid black line is the CFD simulation of the temperature. Solid blue circles are the temperature of the flow retrieved by REMPI spectra of dilute sample of NO and red diamonds represent the temperature of the secondary expansion obtained by the CP-FT mmW spectra of Furan.

nozzle throat. The subsequent drop in intensity is where the dense room-temperature reservoir filled with furan attenuates the photolysis laser through strong absorption.

We determined the pseudo-first-order rate coefficient *k′* after the rise was complete, beginning at ~100 μs. The pseudo-first order decay constant is calculated by fitting the HCO signal to the following,

$$[\mathrm{HCO}]_t = \mathrm{A}\exp(-k't)$$

where $[HCO]_t$ is the time-dependent HCO signal, A is a fitting constant, and t is time. We choose the 100-225 μs time window to fit the data when determining the pseudo-first order rate coefficient. The solid lines plotted in Fig. 12 are the fits obtained from the above equation for the HCO data. The calculated pseudo-first-order rate coefficient was plotted against the O_2 density (Fig. 13) and the slope of the plot is the bimolecular rate coefficient of the reaction, which is found to be 6.66 ± 0.47 × 10^{-11} cm^3 $molec^{-1}$ s^{-1}, roughly twelve times faster than the room temperature rate coefficient[39]. The stated uncertainty is the 95% confidence level from the plot in Fig. 13 with the appropriate *t*-value.

Although there is evidence of reaction prior to the time at which we begin to examine the decay, we have varied this t_0 time and see little dependence on the inferred bimolecular rate as also shown in Fig. 13. Varying the start time for the fits from 90-110 μs gave rate coefficients within the quoted uncertainty. The intercept of the bimolecular rate plot is -3197 ± 239 s^{-1}. This reflects the very slow rise over the sampled window which we attribute to thermalization of vibrationally excited HCO.

The delay between laser firing and the initial rise are a consequence of the distance of the detection region from the nozzle exit and finite width of the probe region. In our previous airfoil sampling paper[35] we discussed the impact of this on the measured rates following a treatment by Taatjes.[55] For supersonic flows, the spread in velocity from the reaction region to the probe region is modest, with little impact on the measured rates. However, the secondary expansion may involve velocity slip of the detected species relative to the overall flow, and this could have an impact on the inferred rate. Simple estimates of the HCO-He velocity slip under our conditions show that velocity slip is negligible[56, 57], owing mainly to the large value of the product of the density and nozzle diameter.

The kinetics of the HCO + O_2 reaction has been studied by experiment at room temperature and above[58-60] and theoretically by Martínez-Ávila et al.[61] and Hsu C.C. et al..[62] In both cases the direct hydrogen

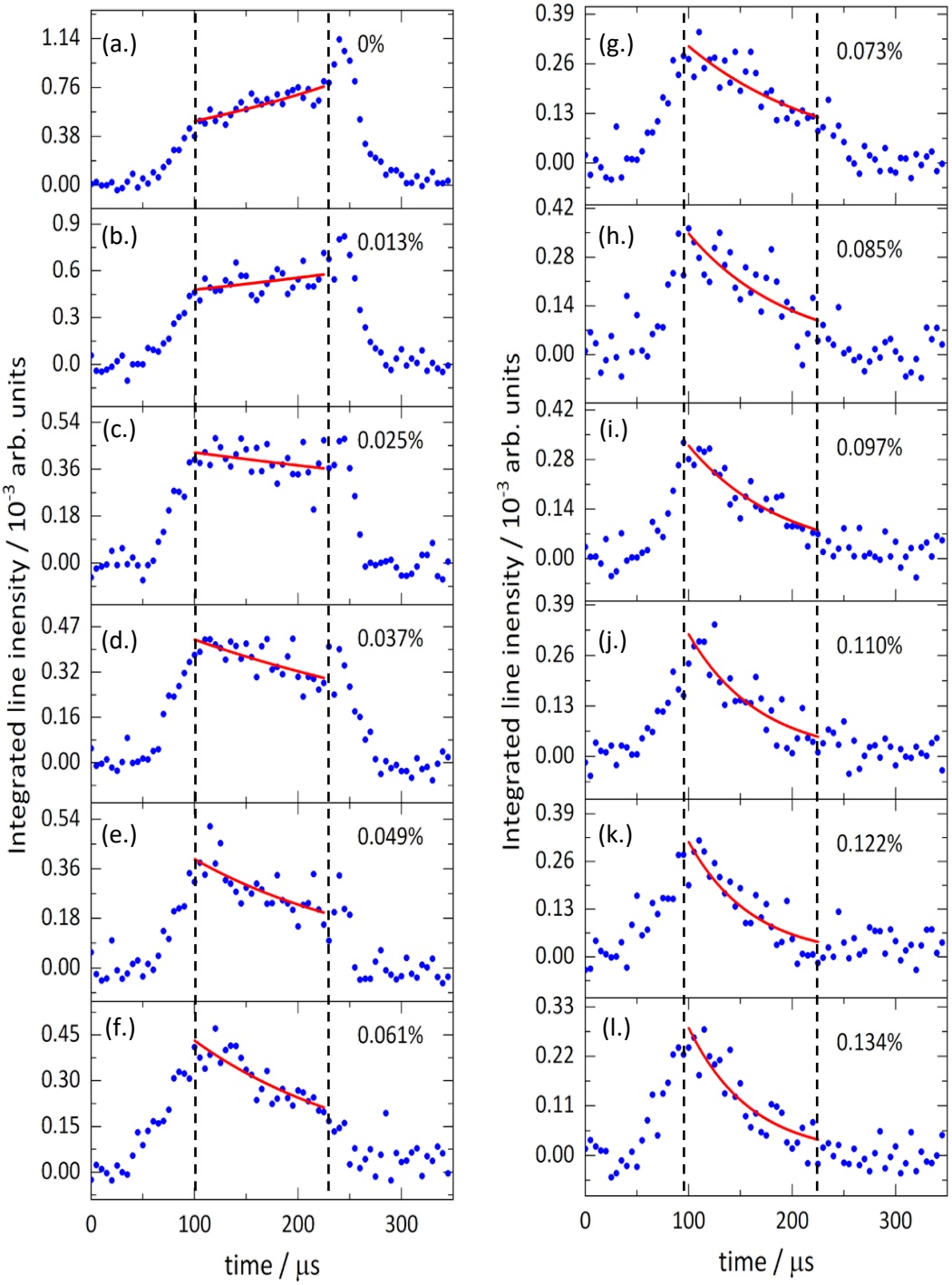

Figure 12. Time- dependent integrated line intensities of HCO 1_{01}-0_{00} line (black filled circles) with increasing O_2 densities. The respective O_2 density is indicated as a percentage of the flow density 2.0 ×10^{17} molecule cm^{-3} at top right. The exponential fit at each O_2 concentration is shown in blue solid lines. The excimer is set to fire at approx. 35 µs after the first chirp and the time window used for the fitting is from 100-225 µs (black dashed lines represent this time window).

abstraction and addition of O_2 has been studied. Hsu et al. examined the direct and indirect pathways

contributing to the reaction and their rates in detail at the G2M(RCC)//B3LYP/6-311G(d,p) level of theory with variational treatment of the barrierless pathway and RRKM calculations. Direct abstraction of H by O_2 was found to be unimportant below 2000 K. Instead, addition of O_2 at the carbon atom forms the long-lived intermediate HC(O)OO, which is 36.1 kcal/mol below the reactant entrance channel. This intermediate may rearrange by H migration over a 5.9 kcal/mol barrier (relative to reactants) to HO_2 + CO or OH + CO_2, or, the more favored path, it may decompose via a loose 4-center transition state 12.6 kcal/mol below reactants to give HO_2 + CO. At low temperatures the latter pathway is dominant. The overall rate of reaction shows a weak negative temperature dependence from 300 to about 450 K and a strong positive temperature dependence above 500 K. The theoretical calculations are in agreement for the experimental data where available.

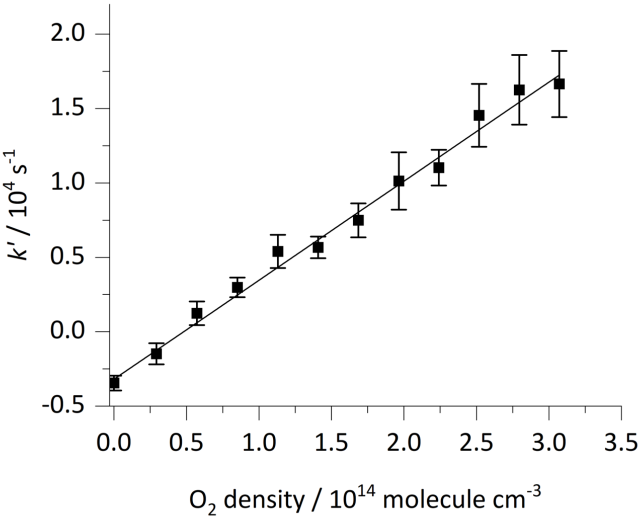

Figure 13. Pseudo-first order rate constant (k′) vs. varying density of O_2.

Conclusion

In this report, we demonstrate the development of an extended Laval nozzle that creates a uniform flow within the nozzle itself then undergoes a shock-free secondary expansion, yielding a low collisional environment suitable for the CP-FTmmW spectroscopic detection. This combination permits use of the CPUF technique for low-temperature kinetics measurements by the CRESU technique. We also demonstrate coupling of a pulsed Laval flow with REMPI detection of a dilute sample of NO. We used 1+1 REMPI with a simple detection scheme in two different flows, one at 33 K and the other at 50 K. The recorded spectra and simulation obtained from LIFBASE were used to determine the flow temperature, which was found to be 30 and 50 K, respectively. We then used REMPI to characterize the flow within the extended nozzle, to avoid the traditional pitot method that could cause interfering shocks. We used a 3D printed split nozzle to house the five cathodes and six anodes. The REMPI measurements show that the flow temperature is 19.7 ± 2.5 K inside the extended nozzle along the axis close to the temperature

retrieved through CFD. We also characterized the secondary expansion using both the 1+1 REMPI of NO and mmWave spectra of furan. We were able to confirm that the temperature in the chosen probe region was around 4 K using both experimental methods and CFD. Finally, we have measured the rate of reaction of HCO + O_2 at 20 K using the extended Laval nozzle developed in this study. We measured the rate to be $6.66 \pm 0.47 \times 10^{-11}$ cm^3 $molec^{-1}$ s^{-1}, many times faster than the room temperature rate but in line with expectations based upon previous characterization of stationary points on the potential energy surfaces.

Acknowledgments

This work was supported by the NSF under award CHE-2247776 and CFD calculations have been performed thanks to CampuStart from Campus Innovation of the University of Rennes.

Conflict of Interest Statement

The authors have no conflicts to declare.

Author Contributions

AGS conceived the experimental methods obtained funding and provided project supervision. NSD conceived the extended Laval nozzle approach and calculated its profile. ST and RG led the investigation with contributions from ME, JL and AB. AGS and ST wrote the original draft with contributions from NSD. NSD performed the CFD simulations.

Data Availability Statement

The data supporting the findings of this article are within the article itself or available from the authors upon reasonable request.

References

[1] B. Rowe, G. Dupeyrat, J. Marquette, and P. Gaucherel, "Study of the reactions N+ 2+ 2N2→ N+ 4+ N2 and O+ 2+ 2O2→ O+ 4+ O2 from 20 to 160 K by the CRESU technique" J. Chem. Phys. **80** (1984) 4915.

[2] I. W. Smith, and B. R. Rowe, "Reaction kinetics at very low temperatures: laboratory studies and interstellar chemistry" Acc. Chem. Res. **33** (2000) 261.

[3] D. B. Atkinson, and M. A. Smith, "Radical-molecule kinetics in pulsed uniform supersonic flows: termolecular association of OH+ NO between 90 and 220 k" J. Phys. Chem. **98** (1994) 5797.

[4] J. J. Ferreiro, S. Chakrabarty, B. Schläppi, and R. Signorell, "Observation of propane cluster size distributions during nucleation and growth in a Laval expansion" J. Chem. Phys. **145** (2016) 211907.

[5] S. Lee, R. J. Hoobler, and S. R. Leone, "A pulsed Laval nozzle apparatus with laser ionization mass spectroscopy for direct measurements of rate coefficients at low temperatures with condensable gases" Rev. Sci. Instrum. **71** (2000) 1816.

[6] S. E. Taylor, A. Goddard, M. A. Blitz, P. A. Cleary, and D. E. Heard, "Pulsed Laval nozzle study of the kinetics of OH with unsaturated hydrocarbons at very low temperatures" Phys. Chem. Chem. Phys. **10** (2008) 422.

[7] B. Hansmann, and B. Abel, "Kinetics in cold laval nozzle expansions: From atmospheric chemistry to oxidation of biomolecules in the gas phase" ChemPhysChem **8** (2007) 343.

[8] J. Daranlot *et al.*, "Revealing atom-radical reactivity at low temperature through the N+ OH reaction" Science **334** (2011) 1538.

[9] S. Soorkia, C.-L. Liu, J. D. Savee, S. J. Ferrell, S. R. Leone, and K. R. Wilson, "Airfoil sampling of a pulsed Laval beam with tunable vacuum ultraviolet synchrotron ionization quadrupole mass spectrometry: Application to low-temperature kinetics and product detection" Rev. Sci. Instrum. **82** (2011).

[10] D. B. Atkinson, and M. A. Smith, "Design and characterization of pulsed uniform supersonic expansions for chemical applications" Rev. Sci. Instrum. **66** (1995) 4434.

[11] I. R. Sims, J.-L. Queffelec, D. Travers, B. R. Rowe, L. B. Herbert, J. Karthäuser, and I. W. Smith, "Rate constants for the reactions of CN with hydrocarbons at low and ultra-low temperatures" Chem. Phys. Lett. **211** (1993) 461.

[12] I. Sims, I. Smith, D. Clary, P. Bocherel, and B. Rowe, "Ultra-low temperature kinetics of neutral–neutral reactions: New experimental and theoretical results for OH+ HBr between 295 and 23 K" J. Chem. Phys. **101** (1994) 1748.

[13] I. Sims, J. Queffelec, A. Defrance, C. Rebrion-Rowe, D. Travers, B. Rowe, and I. Smith, "Ultra-low temperature kinetics of neutral–neutral reactions: The reaction CN+ O2 down to 26 K" J. Chem. Phys. **97** (1992) 8798.

[14] I. Sims *et al.*, "Ultralow temperature kinetics of neutral–neutral reactions. The technique and results for the reactions CN+ O2 down to 13 K and CN+ NH3 down to 25 K" J. Chem. Phys. **100** (1994) 4229.

[15] P. Sharkey, I. R. Sims, I. W. Smith, P. Bocherel, and B. R. Rowe, “Pressure and temperature dependence of the rate constants for the association reaction of OH radicals with NO between 301 and 23 K” J. Chem. Soc. Faraday Trans. **90** (1994) 3609.

[16] R. L. Caravan, R. J. Shannon, T. Lewis, M. A. Blitz, and D. E. Heard, “Measurements of rate coefficients for reactions of OH with ethanol and propan-2-ol at very low temperatures” J. Phys. Chem. A. **119** (2015) 7130.

[17] B. J. Opansky, P. W. Seakins, J. O. P. Pedersen, and S. R. Leone, “Kinetics of the reaction ethynyl radical+ oxygen from 193 to 350 K using laser flash kinetic infrared absorption spectroscopy” J. Phys. Chem. **97** (1993) 8583.

[18] S. Lee, and S. R. Leone, “Rate coefficients for the reaction of C2H with O2 at 90 K and 120 K using a pulsed Laval nozzle apparatus” Chem. Phys. Lett. **329** (2000) 443.

[19] F. Goulay, S. Soorkia, G. Meloni, D. L. Osborn, C. A. Taatjes, and S. R. Leone, “Detection of pentatetraene by reaction of the ethynyl radical (C 2 H) with allene (CH 2 [double bond, length as m-dash] C [double bond, length as m-dash] CH 2) at room temperature” Phys. Chem. Chem. Phys. **13** (2011) 20820.

[20] F. Goulay, D. L. Osborn, C. A. Taatjes, P. Zou, G. Meloni, and S. R. Leone, “Direct detection of polyynes formation from the reaction of ethynyl radical (C 2 H) with propyne (CH 3–C [triple bond, length as m-dash] CH) and allene (CH 2 [double bond, length as m-dash] C [double bond, length as m-dash] CH 2)” Phys. Chem. Chem. Phys. **9** (2007) 4291.

[21] J. O. P. Pedersen, B. J. Opansky, and S. R. Leone, “Laboratory studies of low-temperature reactions of ethynyl with acetylene and implications for atmospheric models of Titan” J. Phys. Chem. **97** (1993) 6822.

[22] S. Lee, D. A. Samuels, R. J. Hoobler, and S. R. Leone, “Direct measurements of rate coefficients for the reaction of ethynyl radical (C2H) with C2H2 at 90 and 120 K using a pulsed Laval nozzle apparatus” J. Geophys. Res.: Planets **105** (2000) 15085.

[23] N. Suas-David, S. Thawoos, and A. G. Suits, “A uniform flow–cavity ring-down spectrometer (UF-CRDS): A new setup for spectroscopy and kinetics at low temperature” J. Chem. Phys. **151** (2019) 244202.

[24] S. Thawoos, G. Hall, C. Cavallotti, and A. Suits, “Kinetics of CN (v= 1) reactions with butadiene isomers at low temperature by cw-Cavity Ringdown in a pulsed Laval flow with theoretical modelling of rates and entrance channel branching” Faraday Disc. **245** (2023) 245.

[25] S. S. Brown, A. Ravishankara, and H. Stark, “Simultaneous kinetics and ring-down: rate coefficients from single cavity loss temporal profiles” J. Phys. Chem. A. **104** (2000) 7044.

[26] J. M. Oldham *et al.*, “A chirped-pulse Fourier-transform microwave/pulsed uniform flow spectrometer. I. The low-temperature flow system” J. Chem. Phys. **141** (2014) 154202.

[27] C. Abeysekera *et al.*, “A chirped-pulse Fourier-transform microwave/pulsed uniform flow spectrometer. II. Performance and applications for reaction dynamics” J. Chem. Phys. **141** (2014) 214203.

[28] G. B. Park, A. H. Steeves, K. Kuyanov-Prozument, J. L. Neill, and R. W. Field, "Design and evaluation of a pulsed-jet chirped-pulse millimeter-wave spectrometer for the 70–102 GHz region" J. Chem. Phys. **135** (2011).

[29] K. Prozument *et al.*, "Chirped-pulse millimeter-wave spectroscopy for dynamics and kinetics studies of pyrolysis reactions" Phys. Chem. Chem. Phys. **16** (2014) 15739.

[30] G. B. Park, and R. W. Field, "Perspective: The first ten years of broadband chirped pulse Fourier transform microwave spectroscopy" J. Chem. Phys. **144** (2016).

[31] D. P. Zaleski, L. B. Harding, S. J. Klippenstein, B. Ruscic, and K. Prozument, "Time-resolved kinetic chirped-pulse rotational spectroscopy in a room-temperature flow reactor" J. Phys. Chem. Lett. **8** (2017) 6180.

[32] B. M. Broderick, N. Suas-David, N. Dias, and A. G. Suits, "Isomer-specific detection in the UV photodissociation of the propargyl radical by chirped-pulse mm-wave spectroscopy in a pulsed quasi-uniform flow" Phys. Chem. Chem. Phys. **20** (2018) 5517.

[33] D. W. Kohn, H. Clauberg, and P. Chen, "Flash pyrolysis nozzle for generation of radicals in a supersonic jet expansion" Rev. Sci. Instrum. **63** (1992) 4003.

[34] H. W. Rohrs, C. T. Wickham-Jones, G. B. Ellison, D. Berry, and B. M. Argrow, "Fourier transform infrared absorption spectroscopy of jet-cooled radicals" Rev. Sci. Instrum. **66** (1995) 2430.

[35] R. M. Gurusinghe, N. Dias, R. Krueger, and A. G. Suits, "Uniform supersonic flow sampling for detection by chirped-pulse rotational spectroscopy" J. Chem. Phys. **156** (2022) 014202.

[36] K. Shibuya, T. Ebata, K. Obi, and I. Tanaka, "Rate constant measurements for the reactions of oxomethyl radical with nitric oxide and molecular oxygen in the gas phase" J. Phys. Chem. **81** (1977) 2292.

[37] J. Reilly, J. Clark, C. B. Moore, and G. C. Pimentel, "HCO production, vibrational relaxation, chemical kinetics, and spectroscopy following laser photolysis of formaldehyde" J. Chem. Phys. **69** (1978) 4381.

[38] A. O. Langford, and C. B. Moore, "Reaction and relaxation of vibrationally excited formyl radicals" J. Chem. Phys. **80** (1984) 4204.

[39] Y. Ninomiya *et al.*, "Cavity ring-down spectroscopy and relative rate study of reactions of HCO radicals with O2, NO, NO2, and Cl2 at 295 K" J. Phys. Chem. A. **104** (2000) 7556.

[40] A. Fein, J. S. Bernstein, X.-M. Song, and T. A. Cool, "Experiments concerning resonance-enhanced multiphoton ionization probe measurements of flame-species profiles" Appl. Opt. **33** (1994) 4889.

[41] J. S. Bernstein *et al.*, "Laser-based flame species profile measurements: a comparison with flame model predictions" Combust. Flame **92** (1993) 85.

[42] J. Luque, "LIFBASE, Database and spectral simulation for diatomic molecules" SRI International Report **99** (1999).

[43] O. Durif *et al.*, “A new instrument for kinetics and branching ratio studies of gas phase collisional processes at very low temperatures” Rev. Sci. Instrum. **92** (2021).

[44] S. Soorkia, C.-L. Liu, J. D. Savee, S. J. Ferrell, S. R. Leone, and K. R. Wilson, “Airfoil sampling of a pulsed Laval beam with tunable vacuum ultraviolet synchrotron ionization quadrupole mass spectrometry: Application to low-temperature kinetics and product detection” Rev. Sci. Instrum. **82** (2011) 124102.

[45] C. B. Cohen, and E. Reshotko, in *National Advisory Committee for* Aeronautics (1956).

[46] J. L. Potter, and W. H. CARDEN, “Design of axisymmetric contoured nozzles for laminar hypersonic flow” J. Spacecraft Rock. **5** (1968) 1095.

[47] H. G. Weller, G. Tabor, H. Jasak, and C. Fureby, “A tensorial approach to computational continuum mechanics using object-oriented techniques” Comp. Phys. **12** (1998) 620.

[48] O. Foundation, https://openfoam.org/version/11/, September 1, 2023

[49] C. M. Western, and B. E. Billinghurst, “Automatic and semi-automatic assignment and fitting of spectra with PGOPHER” Phys. Chem. Chem. Phys. **21** (2019) 13986.

[50] H. S. Müller, F. Schlöder, J. Stutzki, and G. Winnewisser, “The Cologne Database for Molecular Spectroscopy, CDMS: a useful tool for astronomers and spectroscopists” J. Mol. Struct. **742** (2005) 215.

[51] D. Patterson, and J. M. Doyle, “Cooling molecules in a cell for FTMW spectroscopy” Mol. Phys. **110** (2012) 1757.

[52] S. Radhakrishnan, T. Hager, A. Kanaherarachchi, C. Williams, G. Hall, and B. Broderick, “Buffer gas cooled ice chemistry. I. Buffer gas cell and mm-wave spectrometer” J. Chem. Phys. **157** (2022).

[53] J. McGurk, T. Schmalz, and W.-H. Flygare, “A density matrix, Bloch equation description of infrared and microwave transient phenomena” Adv. Chem. Phys. (1974) 1.

[54] O. Sorkhabi, F. Qi, A. H. Rizvi, and A. G. Suits, “Ultraviolet photodissociation of furan probed by tunable synchrotron radiation” J. Chem. Phys. **111** (1999) 100.

[55] C. A. Taatjes, “How does the molecular velocity distribution affect kinetics measurements by time-resolved mass spectrometry?” Int. J. Chem. Kin. **39** (2007) 565.

[56] D. R. Miller, “Free jet sources” in Atomic and Molecular Beam Methods, G. Scoles, D. Bassi, U. Buck, D. C. Laine, Eds. Oxford University Press, **1** (1988) 14.

[57] A. W. Jasper, and J. A. Miller, “Lennard–Jones parameters for combustion and chemical kinetics modeling from full-dimensional intermolecular potentials” Combust. Flame **161** (2014) 101.

[58] A. Matsugi, and A. Miyoshi, “Yield of formyl radical from the vinyl+ O2 reaction” Int. J. Chem. Kin. **46** (2014) 260.

[59] J. D. DeSain, L. E. Jusinski, A. D. Ho, and C. A. Taatjes, “Temperature dependence and deuterium kinetic isotope effects in the HCO (DCO)+ O2 reaction between 296 and 673 K” Chem. Phys. Lett. **347** (2001) 79.

[60] S. Dóbé, H. Wagner, and H. Ziemer, “Rate and stoichiometry of the fast gas titration reaction HCO+ O 2→ CO+ HO 2” React. Kin. Catal. Lett. **54** (1995) 271.

[61] M. Martínez-Ávila, J. Peiró-García, V. c. M. Ramírez-Ramírez, and I. Nebot-Gil, “Ab initio study on the mechanism of the HCO+ O2→ HO2+ CO reaction” Chem. Phys. Lett. **370** (2003) 313.

[62] C. C. Hsu, A. Mebel, and M.-C. Lin, “Ab initio molecular orbital study of the HCO+ O2 reaction: Direct versus indirect abstraction channels” J. Chem. Phys. **105** (1996) 2346.